RailCloud-HdF: A Large-Scale Point Cloud Dataset for Railway Scene Semantic Segmentation

Mahdi Abid[a], Mathis Teixeira, Ankur Mahtani*[b] and Thomas Laurent
FCS Railenium, F-59300 Famars, France

Keywords: Point Cloud Dataset, Railway Scenes, Semantic Segmentation, Deep Learning, LiDAR.

Abstract: Semantic scene perception is critical for various applications, including railway systems where safety and efficiency are paramount. Railway applications demand precise knowledge of the environment, making Light Detection and Ranging (LiDAR) a fundamental component of sensor suites. Despite the significance of 3D semantic scene understanding in railway context, there exists no publicly available railborne LiDAR dataset tailored for this purpose. In this work, we present a large-scale point cloud dataset designed to advance research in LiDAR-based semantic scene segmentation for railway applications. Our dataset offers dense point-wise annotations for diverse railway scenes, covering over 267km. To facilitate rigorous evaluation and benchmarking, we propose semantic segmentation of point clouds from a single LiDAR scan as a challenging task. Furthermore, we provide baseline experiments to showcase some state-of-the-art deep learning methods for this task. Our findings highlight the need for more advanced models to effectively address this task. This dataset not only catalyzes the development of sophisticated methods for railway applications, but also encourages exploration of novel research directions.

1 INTRODUCTION

3D data are crucial for environment perception, and substitute images in various applications e.g. urban mapping, autonomous cars. The most common form of such data is point clouds with 3D coordinates and associated radiometry information. Different machine vision methods have been applied to the environment recognition and visualization using three-dimensional data, especially in different areas of robotics, e.g. laser scanning system (Sergiyenko et al., 2023). However, these methods usually result in a contradiction between data processing time and obtained performance. As a result, deep-learning-based techniques have attracted considerable attention recently, inspired by their powerful capacity in other fields (Abid and Lefebvre, 2021; Compagnon et al., 2023). As deep learning for image processing has already developed towards industrial use, deep learning for 3D point cloud processing remains an ongoing field of research. Regarding the application of deep learning methods for point cloud analysis, the main tasks include semantic segmentation (Guo et al., 2021). In recent years, the autonomous car industry has played a crucial role in its development, particularly by providing open source data e.g. SemanticKITTI (Behley et al., 2019).

With the growing embeddability and reduced cost of LiDAR (Light Detection And Ranging) scanners, point cloud data for large-scale geomatics become widely available, e.g. the OpenTopography[1] database. Several high-density open source LiDAR datasets, e.g. Hessigheim Benchmark (Kölle et al., 2021), address the issue of Point Cloud Semantic Segmentation (PCSS) i.e. providing a label to each point based on the object or structure to which it belongs. Although this information is low-level, it is used to build meaningful representations for real-world applications like vegetation mass estimate and infrastructure cartography (Soilán et al., 2019). Deep-learning-based processing is at its early stages of development in the railway field. Point cloud semantic information could simplify existing use cases and lead to new railway applications e.g. condition estimate of level crossing barriers, automated site inventory, etc. Reliable railway LiDAR PCSS marks an initial step towards optimizing maintenance.

[a] https://orcid.org/0000-0001-5504-3014
[b] https://orcid.org/0000-0003-2738-4705
*Corrresponding author

[1] https://opentopography.org

Abid, M., Teixeira, M., Mahtani, A. and Laurent, T.
RailCloud-HdF: A Large-Scale Point Cloud Dataset for Railway Scene Semantic Segmentation.
DOI: 10.5220/0012394800003660
Paper published under CC license (CC BY-NC-ND 4.0)
In *Proceedings of the 19th International Joint Conference on Computer Vision, Imaging and Computer Graphics Theory and Applications (VISIGRAPP 2024) - Volume 2: VISAPP*, pages 159-170
ISBN: 978-989-758-679-8; ISSN: 2184-4321

In this paper, we address the issue of lack of accessible LiDAR data in railway sector, which are crucial for empirical evaluation of approaches dedicated to tasks in railway applications. We propose RailCloud-HdF[2], a large-scale LiDAR point cloud dataset with point-wise annotation of railway scenes. Compared to other railway point cloud datasets mentioned in literature, our dataset is the largest one with a relatively good precision, and to the best of our knowledge, it is the first in railway category to be made publicly available. We consider semantic segmentation of point clouds from a single LiDAR scan as a task for our dataset benchmarking. To address this task, training and evaluation of deep-learning-based state-of-the-art approaches is performed using splits from our dataset. The paper is organized as follows: we first introduce works related to the topic, along with our dataset. Then, we present the choice of our baseline methods, and explain the methodology developed for the segmentation task. Afterwards, we discuss our segmentation results, speed and robustness to point density. We finally detail some future research directions.

2 RELATED WORK

This section is devoted to the presentation of recent works related to the methods and domain of our study. These works can be divided into three main categories: (1) Existing 3D LiDAR point cloud datasets, (2) Railway LiDAR PCSS, and (3) Deep learning methods for LiDAR PCSS.

2.1 Existing Datasets

Datasets are essential for empirical assessment of studied approaches. When they are publicly available along with benchmarks, they serve two primary functions: firstly, they establish a foundation for tracking progress, as they enable the presentation of results that can be reproduced and assessed against each other, and secondly, they facilitate the creation of innovative methods without the initial costly task of gathering and annotating data. Although there are several datasets designed for image-based semantic segmentation (Neuhold et al., 2017; Cordts et al., 2016), the availability of datasets featuring point-wise annotations for 3D point clouds remains relatively limited. Table 1 shows recent examples, which can be categorized into urban datasets generally proposed for self-driving car applications, and railway datasets used for mobile mapping systems or environment monitoring tasks.

Among the railway datasets, one can cite Saint-Etienne dataset which is a LiDAR point cloud dataset acquired in industrial settings to illustrate performances of a novel deep-learning-based method for 3D PCSS. Other examples are the datasets used in (Grandio et al., 2022) to test a methodology that segments both punctual and linear elements from railway infrastructure. The most notable difference between these datasets and those from urban environments is that they are not made publicly available, which highlights the gap between the two sectors in terms of availability of data acquired using LiDAR sensors.

2.2 Railborne LiDAR PCSS

In the railway industrial context, standard model-based methods often rely on user-implemented global and local geometrical features and trajectory information, and are usually object-oriented (Lamas et al., 2021). While these methods tend to perform well in controlled environments, they need to be refined for any use case changes and are sensitive to unanticipated features.

In a recent study conducted by Guinard et al. (Guinard et al., 2021), a fast random forest classifier is introduced, which relies on a set of handcrafted features derived from eigenvalues of local point-neighborhood covariance matrices. To enhance the algorithm's robustness to ill-sampled data and to speed up the process, the authors have developed a pre-segmentation step, partitioning the point cloud into geometrically homogeneous segments for subsequent classification, which is then propagated back to the original cloud.

Exploring deep-learning methods, Soilán et al. (Soilán et al., 2020) apply PointNet (Qi et al., 2017a) and KPConv (Thomas et al., 2019) methods to segment point cloud data from railway tunnels. Despite the simplicity of the test environment, their research has revealed promising outcomes in the context of thorough infrastructure segmentation. In a similar vein, Manier et al. (Manier et al., 2022) introduce a deep-learning-based approach for 3D PCSS tailored for LiDAR captured railway scenes. It relies on local point cloud transformations for convolutional learning, and effectively extracts useful information for maintenance and topological analysis, while demonstrating remarkable robustness against variations in point distribution and redundancy.

[2] The dataset can be downloaded from: railenium_sharepoint_mahtani
For any queries, please contact: mahdiabid91@gmail.com

Table 1: Overview of recent urban and railway point cloud datasets with point-wise semantic annotation. Missing information is not mentioned in the corresponding references. [1] Total number of points given in millions, [2] Number of classes used for evaluation and number of annotated classes in brackets, [3] Total distance covered by the sensor during data acquisition in km, [4] Length of tiles in which the entire point clouds are subdivided, [5] Range precision which is the maximum distance separating two contiguous points, [6] Number of points per m^2 (average value or range), [7] (Vallet et al., 2015), [8] (Hackel et al., 2017), [9] (Roynard et al., 2018), [10] (Behley et al., 2019), [11] (Manier et al., 2022).

Dataset	#points[1]	#classes[2]	length[3]	tile[4]	precision[5]	density[6]	sensor	published
IQmulus[7]	12	22 (22)	0.21	-	-	-	Riegl LMS-Q120i	✓
(Zhang et al., 2015)	32	10 (10)	-	-	-	-	Velodyne HDL-64E	✓
Semantic3d[8]	4009	8 (8)	-	-	-	-	Terrestrial Laser Scanner	✓
Paris-Lille-3D[9]	143.1	9 (50)	1.94	-	-	1000-2000	Velodyne HDL-32E	✓
SemanticKITTI[10]	4549	25 (28)	-	100m	-	-	Velodyne HDL-64E	✓
(Lamas et al., 2021)	>3000	10 (10)	90	200m	5mm	980	Lynx Mobile Mapper	✗
(Grandio et al., 2022)	39	-	2	-	30mm	644	G_lidar	✗
(Grandio et al., 2022)	129	-	0.4	200m	5mm	11000	RIEGL LiDAR	✗
Saint-Etienne[11]	257	9 (9)	13	-	-	-	-	✗
RailCloud-HdF	8060.3	8 (9)	267.52	50m	7mm	2400	RIEGL VUX-1HA	✓

2.3 Deep Learning Methods for LiDAR PCSS

Irrespective of the lack of implemented deep learning approaches for PCSS in railway context, the design and application of such approaches to general purposes have been significantly growing over the recent years. Indeed, due to the very broad range of approaches adopted in this area, it is useful to divide them into different categories.

Projection-based methods in LiDAR PCSS operate by first generating images by projecting the 3D point cloud onto a 2D plane. Convolutional Neural Networks (CNNs) are then applied to these images to perform segmentation, and the result is projected back onto the original point cloud. A well-known method is RangeNet++ (Milioto et al., 2019), which projects 3D points onto a 2D spherical grid. One notable advantage is that CNNs are known to yield state-of-the-art results for image-based tasks. However, projection-based methods are sensitive to the choice of viewpoint for generating images, which can lead to inconsistencies in segmentation results. Moreover, they may not fully exploit the entire geometric information present in point cloud data.

Discretization-based methods aim to transform the unordered and sparse LiDAR point clouds into structured 3D grids, often using a process called voxelization. This transformation enables the application of 3D-CNNs, the 3D equivalent of traditional 2D-CNNs used for image data. However, voxelization introduces memory and precision constraints, as the memory usage grows cubically with the point cloud size, making these methods unsuitable for large-scale data. To mitigate memory usage, sparse representations ignoring empty cells have been introduced with Minkowski CNN (Choy et al., 2019). While these techniques improve memory efficiency, they may still struggle with extremely large-scale point clouds.

Point-wise methods operate directly on raw coordinates. PointNet (Qi et al., 2017a), the pioneer of these methods, applies Multi Layer Perceptron (MLP) to individual points to extract features, providing a foundation for subsequent approaches. PointNet++ (Qi et al., 2017b) introduces hierarchical feature learning from larger to local regions, which enhances its robustness. RandLA-Net (Hu et al., 2020) addresses the challenge of large-scale point clouds by adopting random sampling and local feature aggregation, although it may suffer from reduced accuracy due to this sampling strategy. KPConv (Thomas et al., 2019) proposes Kernel Point Convolutions, which determine convolution weights based on Euclidean distances to points, offering a novel approach to extracting local structures efficiently. Expanding on this kernel-based approach, ConvPoint (Boulch, 2020) takes it a step further by replacing discrete kernels with continuous ones, further refining the technique for local structure extraction. These point-wise methods excel in preserving the original point information, which is beneficial for maintaining detailed geometry in the segmentation process. However, they may struggle with inefficient local context extraction.

Table 2: Specifications of data acquisition systems.

Laser Scanner	RIEGL VUX-1HA
INS system	IGI Compact MEMS (ROBIN)
GNSS receiver	Septentrio Dual GNSS
Camera	FLIR Grasshopper 3 12MP camera - CX-Format CMOS

3 THE RailCloud-HdF DATASET

3.1 Data Acquisition

In order to collect railway point cloud data, two identical systems[3] combining LiDAR technology with an accurate and lightweight INS (Inertial Navigation System) were used. Each system integrates a laser scanner with a field angle view of 360°, an acquisition rate of 200Hz and 1mm precision within a range of 119m around the surveying wagon. It also integrates a 12MP camera, two GNSS (Global Navigation Satellite System) antennas, a GIS (Geographic Information System) quality IMU (Inertial Measurement Unit) navigation system, a touch screen control unit, and three mounting systems. System specifications are given in Table 2.

The two systems were installed on a railborne flat wagon as shown in Figure 1(a). The systems were mounted horizontally on the top of the wagon by means of a mounting frame, and at a height of 3.61m as if it were positioned on both sides of a train front at the level of the driver's cab (cf. Figure 1(b)). The mounting frame is equipped with damping devices capable of resisting the weight of the system and all other forms of load in order to limit the vibrations and torsion effects of the acquisition device and to ensure the quality of data. The device is equipped with a long-life battery that allows it to be autonomous during the entire acquisition sequence. Its autonomy enables to cover about 350km of tracks at 60km/h on average over a day.

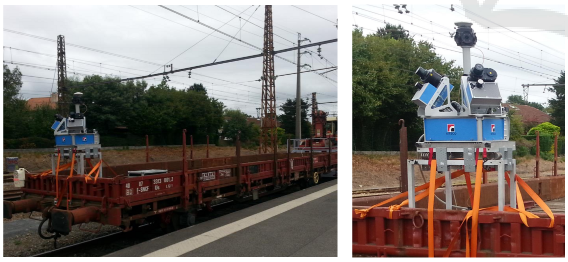
(a)

(b)

Figure 1: Experimental platform: (a) overview of the wagon, (b) acquisition device.

A large amount of LiDAR point cloud data was acquired from eight railway lanes connecting 11 cities in the *Hauts-de-France* region in northern France, hence the suffix "HdF" added to the dataset name. The connected cities are *Aulnoye*, *Busigny*, *Lille*, *Douai*, *Lens*, *Ostricourt*, *Don*, *Bethune*, *Hazebrouck*, *Calais* and *Dunkerque*. The railway lanes are 267.52km long in total. To further densify the obtained point clouds, the travels on the eight lanes were conducted in round trip. In order to obtain quality data, the acquisitions were carried out in adequate meteorological conditions (absence of rain and fog) and sufficient light conditions (acquisition during the day). The acquisitions guarantee a minimum density of one point every 5cm per scan by combining both passes of round trip, on a corridor of 20m centered on the acquisition system (10m on both sides), regardless the measured surface and the wagon velocity. Data acquisition on the different lanes took place in the interval of four days.

3.2 Annotation Process

For point-wise annotation, manual segmentation in 3D was performed tile by tile using *CloudCompare* software (version 2.12.2) (CloudCompare, 2022). In order to obtain consistent, geometrically reliable and correct labels, annotators rely on the colorized point clouds. Color channels are the result of adjusting the images acquired by the cameras to the point clouds.

Annotating 3D point clouds is laborious since the annotator often has to adjust the viewpoint. On average, an annotator needs 1.5 hours per tile. Each tile labels are also verified by a different annotator, which adds 10 minutes on average per tile.

3.3 Dataset Format

Acquired LiDAR point data records are contained in compressed LAS files (.laz extension) of version LAS 1.2 and point data format type 3. This format stores 3D coordinates, intensity, classification and color channels, with the addition of GPS time.

Table 3: Statistics related to point cloud data collected for each of the eight railway lanes. [1] Name of railway lane in departure-arrival format, [2] Total number of points given in millions, [3] Distance covered by the sensor during data acquisition in km, [4] Number of tiles in which the acquired point clouds are subdivided.

Railway lane[1]	#points[2]	length[3]	#tiles[4]
Aulnoye-Busigny	1051.2	34.62	693
Lille-Douai	1496	43.01	861
Lens-Ostricourt	424.7	14.78	296
Don-Lens	435.4	16.13	323
Don-Bethune	686.8	23.09	463
Lille-Don	873	27.63	553
Hazebrouck-Calais	1689.1	60.73	1215
Hazebrouck-Dunkerque	1404.2	47.53	949
Total	8060.3	267.52	5353

[3] The data acquisition systems are made by GEOSAT: https://www.geo-sat.com/fr/moyens-materiels-logiciels/

3.4 Dataset Statistics

The resulting point clouds, saved each in a .laz file, have an average of 1.5 million points. So, more than 8 billion points are comprised in the complete dataset. Some files have many millions of points while the majority of files contain nearly one million points. This is due to the fact that the density of points depends on the geometrical properties of the captured environment, as well as the velocity of the wagon. The files representing a large number of points correspond to the phases when the train is close to the departure or arrival stations, because of the complexity of the station infrastructures and the low speed of the wagon during these phases. Point cloud data statistics per lane are shown in Table 3.

The number and percentage of points belonging to each class are shown in Figure 2. The *ground*, *vegetation* and *unclassified* classes are the most frequent classes. The level crossing gate (*LCG*) class is weakly represented in the dataset since the wagon rarely encounters a level crossing during its travel, but still more than 860 thousand points are labeled.

For datasets collected in natural environments, the distribution of classes is commonly unbalanced, and some classes corresponding to objects or structures that rarely occur are always under-represented. Overall, the unbalanced class distribution is quite comparable in other datasets, e.g. SemanticKITTI (Behley et al., 2019) and Saint-Etienne (Manier et al., 2022).

4 EVALUATION OF SEMANTIC SEGMENTATION

In this section, the evaluation of some state-of-the-art methods for scene semantic segmentation exploiting information of a single scan is depicted.

As the class *unclassified* includes outliers, other structures and objects, and is then too diverse with a high intra-class variation, we decided not to include it in the performance evaluation. Thus, eight instead of nine classes are taken into account during training and testing phases.

4.1 Baseline Approaches

Given the strengths and limitations of different categories of state-of-the-art methods presented in Section 2.3, we choose to use four point-wise architectures to provide results on our dataset. We consider PointNet and its improved version PointNet++, which have been widely tested across the existing literature. We distinguish two versions of PointNet, where PointNet (Vanilla) is the one in (Qi et al., 2017a) that does not use transformation networks. For PointNet++ as well, we test two versions, where PointNet++ (MSG) (Qi et al., 2017b) is the network that applies multi-scale grouping followed by according PointNets to extract features at different scales. Another point-wise MLP method that we test is RandLA-Net (Hu et al., 2020). We finally add a convolution-based architecture which is ConvPoint (Boulch, 2020) that was recently used as a baseline in (Manier et al., 2022) for PCSS in both railborne and airborne LiDAR datasets.

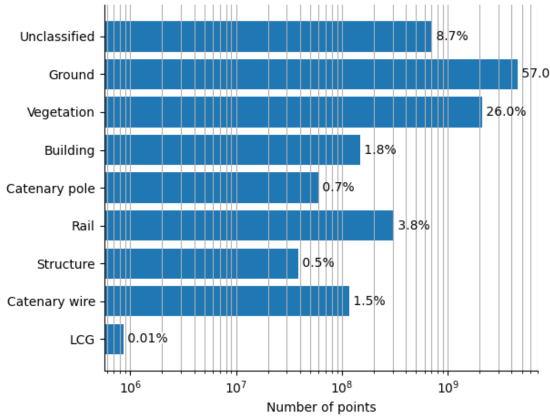

Figure 2: Class distribution. The number and percentage of labeled points per class are shown.

Note that for these baseline networks, we consider the same architectures and hyperparameters as described in the corresponding references. One exception is that for RandLA-Net, point clouds are downsampled with a five-fold decimation ratio and the number of nearest points is set as 32.

4.2 Input and Output of the Methods

In PCSS, per-point classification has been extensively studied (Kaijaluoto et al., 2022). Since there are several attributes to characterize each point of a 3D cloud, the input features that are fed to the networks have to be declared. Hence, in this work, Euclidian coordinates along with intensity values are considered, having as input matrix $\boldsymbol{X} \in \mathbb{R}^{N\times 4}$:

$$\boldsymbol{X} = \begin{bmatrix} \boldsymbol{x} & \boldsymbol{y} & \boldsymbol{z} & \boldsymbol{I} \end{bmatrix} = \begin{bmatrix} x_1 & y_1 & z_1 & I_1 \\ \vdots & \vdots & \vdots & \vdots \\ x_N & y_N & z_N & I_N \end{bmatrix} \tag{1}$$

Where N is the number of input points, (x_i, y_i, z_i) and I_i, i=1,...,N, correspond to the Euclidean coordinates and the intensity value of each point, respectively.

Then, the used deep-learning-based methods aim to estimate the class of each input point of the cloud.

4.3 Preprocessing

Once the input features are defined, preprocessing steps are applied to the point clouds for training phase. These steps are the following:

- **Grid Sampling.** The density of points varies depending on the scanned environment, and the velocity of the wagon when surveying. This makes mandatory the capability of processing point clouds with different point densities. In order to alleviate the task to a neural network, all the point clouds are first subsampled using grid subsampling. The used grid size is 15cm;
- **Cube Crop.** To provide a homogeneous point cloud size to a neural network, it is fed by cubes of 10m each side. During training, only one cube from each scan is sampled in each epoch. For this purpose, a random point of the original scan is taken, and the cube around that point is sampled. With this, different sub-clouds are fed from the same cloud at different epochs;
- **Scale Intensity.** Intensity data are represented as integers, and the LiDAR has 16-bit scanner, then the largest value allowed is 65535. Using this value as a scale factor, intensity data are normalized to [0,1];
- **Scale Coordinates.** The coordinates of the point clouds are usually high, and having high input values may cause instability while training neural networks. To avoid this issue, once a cube is taken, its coordinates are scaled to [0,1] in all axes, using the 10m as the scale factor;
- **Data Augmentation.** The data augmentation consists of duplicating and applying geometric transformations to cubes from the training set that have points labeled as *LCG*, *catenary pole* or *structure*, which are the least represented classes. Cubes containing those objects have been replicated, rotated, cropped each around its barycenter, and Gaussian noise of 2×10^{-3} standard deviation is applied to their point features. To avoid segmentation dependency on the orientation of the railway track, the training cubes were randomly rotated around z-axis, where the maximum rotation is restricted to 180°. With this, the number of points with those labels is incremented and more variability in the training data helps the network to generalize better afterwards;
- **Fixed Number of Points.** Since the considered architectures need to be fed always by a given number of points, the cube points are randomly duplicated or subsampled with replacement to N points. N must be big enough to be representative of the cloud, but the smaller it is, the faster the network will process. We consider N=8192 points.

4.4 Training Details

The dataset need to be split for training, validation, and testing of the models. The scans are shuffled, with 95% used for the training process and the remaining 5% reserved for testing. The training process scans are in their turn split into 80% for model training and 20% for validation. The training process minimizes cross entropy loss between the point labels relative to cubes cropped from training scans and their estimates. As the labels present in the dataset are clearly unbalanced, a loss weighting coefficient is applied allowing stronger error back-propagation for the least populated classes: $\rho = \sqrt[2.5]{\frac{P_{max}}{P_c}}$, $\forall c \in C$ the classes, with P the percentage of points belonging to a class within the training dataset.

The training set is decomposed in batches of eight sequences, and from the 50th epoch, early stopping method is used to end each training process if the validation loss doesn't improve for 20 consecutive epochs. Adam optimizer is used with an initial learning rate of 1×10^{-3}. The maximum number of training epochs is set to 300, and for the first five epochs, a gradual warmup strategy that linearly increases the learning rate from 0 to the initial learning rate is adopted to avoid numerical instability and very slow convergence to the final solution (Goyal et al., 2017). For the next epochs, a cosine learning rate decay (He et al., 2019) is used to decrease the learning rate from the initial value to 0 by following the cosine function, which potentially improves the training progress.

The training is implemented using PyTorch library, and the used hardware consists of an NVIDIA RTX A6000 GPU with 48GB GDDR6 memory and CUDA toolkit 10.1.

As explained in Section 4.2, the intensity is one of the inputs. It is interesting to study whether this feature has a significative impact on the segmentation performance or if it is worth not relying on it to perform well on the task. In consequence, for each of the baseline networks, training is performed using and obviating intensity values to compare both results obtained in the testing phase.

4.5 Performance Evaluation Metrics

To evaluate the results in our study, the metrics used are common for semantic segmentation task, both for image and three-dimensional data. These metrics are the following (Everingham et al., 2015):

- Overall accuracy (OA): It measures the rate of correctly classified points over all points, irrespective of their classes. The more unbalanced data is present in the dataset, the less significative this criterion is;
- Mean accuracy (MA): Unlike OA, this metric considers the accuracies of all classes and calculates their mean value;
- Intersection over Union (IoU): It represents the number of common points between the label and prediction masks, divided by the number of all points present across both masks. It is given by the following equation:

$$\mathrm{IoU} = \frac{\mathrm{TP}}{\mathrm{TP}+\mathrm{FP}+\mathrm{FN}} \tag{2}$$

  where TP, FP and FN are respectively the number of true positive, false positive, and false negative predictions;
- Mean IoU (mIoU): This metric considers the IoUs of all classes and calculates their mean value as follows:

$$\mathrm{mIoU} = \frac{1}{N_c}\sum_{c=1}^{N_c}\frac{\mathrm{TP}_c}{\mathrm{TP}_c+\mathrm{FP}_c+\mathrm{FN}_c} \tag{3}$$

  where TP_c, FP_c and FN_c are respectively the number of true positive, false positive, and false negative predictions for the c^{th} class, and N_c corresponds to the number of classes.

4.6 Testing Results

Once the baseline networks are trained, they are tested against the test tiles. The difference between the testing and training processes is mainly the data pre-processing. A graphical summary of the inference steps undergone by test scans is presented in Figure 3. First, each point cloud is grid-subsampled. Then a grid of resolution 10m is applied to get cropped cubes, which features are scaled, and from which N points are considered. Finally, these fully processed cubes are fed to the network, and its predictions are obtained for final segmentation result. Then, the results are compared to the ground truth of testing data to calculate the metrics.

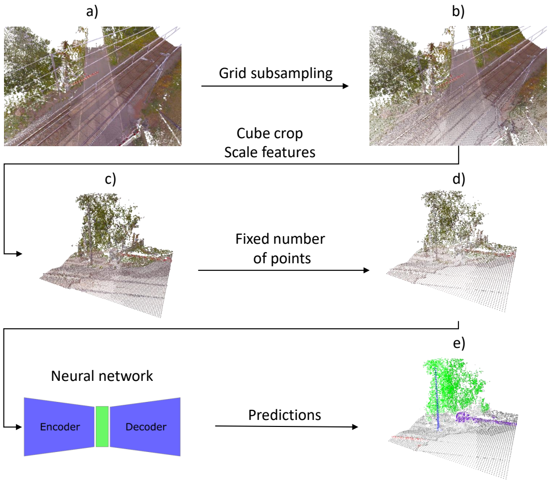

Figure 3: A graphical summary of processing steps involved in the testing phase. (a) raw point cloud, (b) subsampled point cloud, (c) cropped cube, (d) processed cube, (e) prediction result.

4.6.1 Analysis of Semantic Segmentation Performance

Test clouds are completely predicted for segmentation to calculate the metrics shown in Table 4. In the first place, when using intensity values as input, the networks provide much more accurate segmentation, except for RandLA-Net and ConvPoint where the gap in overall and mean metrics is not significant between both intensity use cases. In addition, ConvPoint provides the best accuracy and IoU metrics when only considering 3D point coordinates. Specifically, for level crossing barriers, intensity range is high due to their particular surfaces. Then, this feature helps to better distinguish *LCG* objects from other classes, which is reflected for all networks in a considerable improvement in *LCG* IoU values when using intensity feature.

Regarding the test mIoU metric, while the most performing approaches have values around 75%, this metric drops for PointNet versions and RandLA-Net. As for the IoU values obtained for each class, it is clear that the main issues are *structure* and *LCG*. Since the presence of objects belonging to those classes in the dataset is low, small errors reduce more significantly the IoU. PointNet versions and RandLA-Net mostly underperform while segmenting the least represented objects, and in particular, PointNet versions underperform while segmenting classes without a dominant vertical component (i.e. *ground*, *vegetation* or *rails*). This result supports the fact that PointNet cannot capture the local structural information between points which can be essential for semantic segmentation tasks, and the

Table 4: The testing results obtained for all baselines. Overall accuracy, mean accuracy, mIoU and IoU metrics for each asset are presented. For both intensity feature use cases, the best values of different metrics across the networks are bolded.

			Class IoU			
Network	OA	MA	Ground	Vegetation	Building	Catenary pole
Intensity	IoU	mIoU	Rail	Structure	Catenary wire	LCG
PointNet (Vanilla)	87.11%	77.47%	73.24%	83.49%	63.84%	38.95%
Yes	77.17%	54.84%	45.25%	36.52%	78.74%	18.73%
PointNet	89.20%	75.74%	77.49%	85.73%	67.98%	48.50%
Yes	80.50%	57.01%	53.91%	21.39%	79.45%	21.61%
PointNet++	93.08%	**87.83%**	84.14%	91.47%	80.80%	75.34%
Yes	87.06%	72.63%	52.33%	**51.16%**	96.07%	49.70%
PointNet++ (MSG)	93.98%	87.80%	86.10%	**92.57%**	**82.02%**	**79.89%**
Yes	88.64%	**74.85%**	57.18%	47.42%	**96.17%**	**57.49%**
RandLA-Net	91.64%	81.72%	83.73%	89.95%	65.33%	59.03%
Yes	84.58%	59.97%	66.77%	21.56%	69.31%	24.05%
ConvPoint	**94.01%**	86.98%	**86.48%**	91.69%	81.27%	75.91%
Yes	**88.70%**	74.38%	**75.52%**	41.14%	93.50%	49.53%
PointNet (Vanilla)	82.27%	54.14%	70.12%	77.22%	34.98%	26.89%
No	69.88%	37.68%	13.16%	16.74%	61.31%	01.02%
PointNet	84.76%	66.11%	74.51%	80.52%	40.92%	34.79%
No	73.55%	43.58%	28.92%	19.41%	66.95%	02.61%
PointNet++	92.93%	85.37%	83.83%	91.45%	79.99%	72.74%
No	86.79%	67.97%	50.65%	43.22%	94.09%	27.81%
PointNet++ (MSG)	93.77%	84.40%	86.08%	**92.34%**	**81.61%**	**81.55%**
No	88.26%	68.22%	56.19%	25.75%	**94.19%**	28.04%
RandLA-Net	91.66%	82.55%	85.26%	88.62%	60.38%	55.04%
No	84.60%	59.07%	69.13%	27.19%	82.94%	04.01%
ConvPoint	**94.01%**	**87.43%**	**86.58%**	91.80%	79.70%	76.56%
No	**88.70%**	**73.05%**	**75.96%**	**47.69%**	90.90%	**35.22%**

fact that RandLA-Net is better suited for large-scale point clouds than 10m-size cubes. Also, it is interesting how *structure* objects perform better with the approaches that provide the worst general results.

The best class IoU metrics are achieved by either PointNet++ (MSG) or ConvPoint, except for *structure* IoU which best value (51.16%) is obtained with PointNet++ when using intensity feature. Overall, the results demonstrate how different architectures perform better for different objects.

To gain a deeper insight into the limitations associated with the metrics, we display comparative views of the segmented point clouds for a sample test scan in Figure 4. For the sake of clarity, we have omitted PointNet (Vanilla) and PointNet++ from this illustration, as these are the least performing versions of their networks. First, we notice that for our baseline, considering the intensity significantly enhances segmentation quality, except for RandLA-Net where an inverse trend is observed. In fact, with intensity, RandLA-Net confuses the *structure* class with *building* and *ground* ones. Second, PointNet shows confusion between *rail* and *ground* classes while other approaches do not. This is most likely due to its limited ability to capture fine-grained patterns. Besides, for most cases, and despite their low occurence in the training data, *LCG* objects are completely segmented, but the few predicted false positives drastically decrease the class IoU. Finally, ConvPoint and PointNet++ (MSG) seem to be less sensitive to spatial noise while segmenting objects near the vegetation, such as catenary poles and wires, LCG bases, and buildings.

4.6.2 Processing Speed and Robustness to Point Density

The results of our baseline experiments show that the current state of the art for PCSS falls short for the size and complexity of our dataset. This is caused by the limited capacity of the tested networks, since their number of parameters (see Table 5) is much lower compared to leading image-based semantic segmentation architectures.

PointNet++ versions provide better results than PointNet ones, yet they show longer training time per epoch, attaining more than five times that of PointNet. For PointNet++ and PointNet++ (MSG), the inference time on a single scan is at least twice and three times that of PointNet, respectively. It's worth noting that the MSG version is more expensive than PointNet++ due to the multi-scale region feature extraction. Compared to PointNet++ versions, using RandLA-Net results in a higher inference time, while delivering lower segmentation performance. Although ConvPoint and PointNet++ (MSG) provide quite similar results, ConvPoint shows a 62% decrease in average training epoch time,

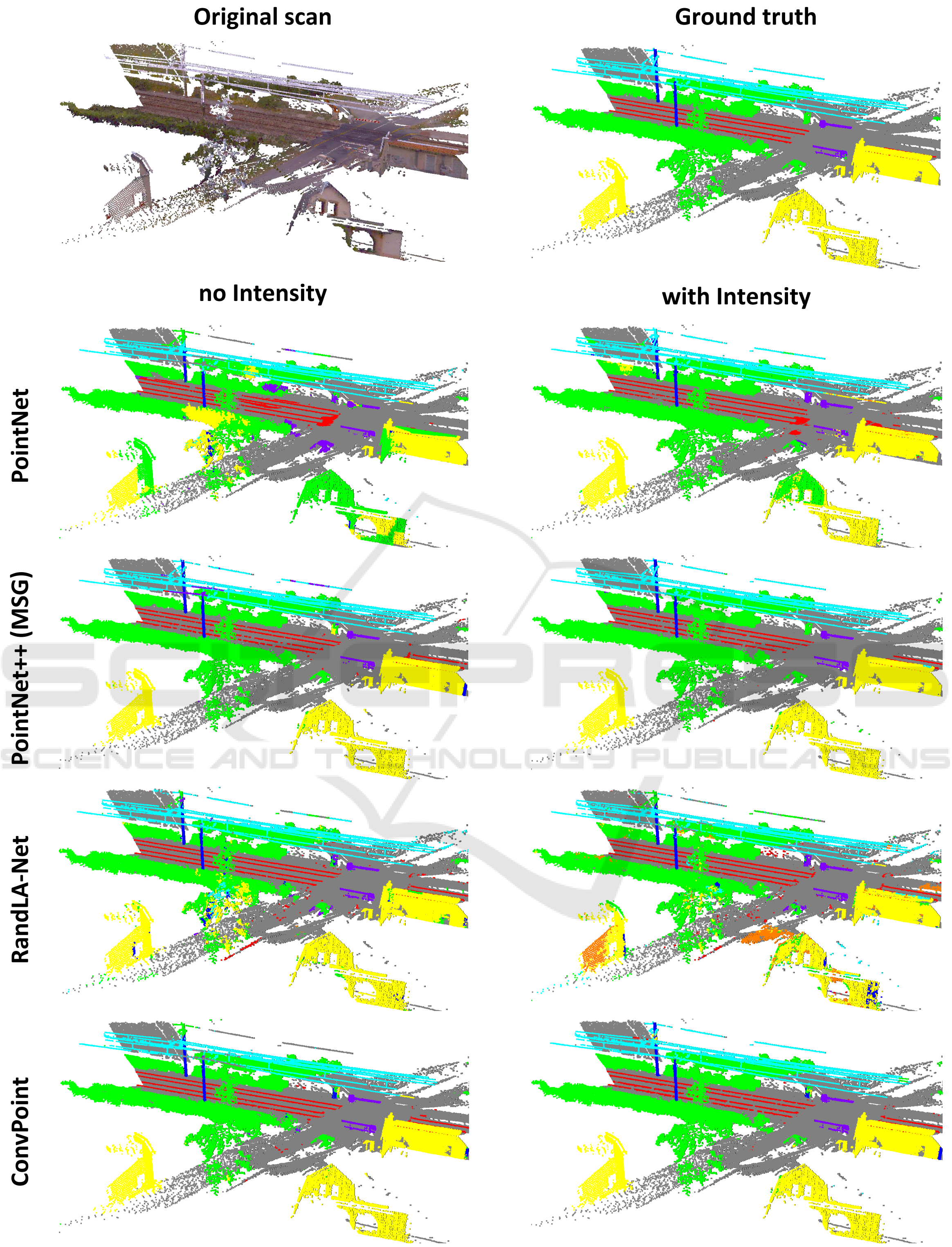

Figure 4: Qualitative segmentation results on a sample test scan, with *ground* in grey, *vegetation* in green, *building* in yellow, *catenary pole* in blue, *rail* in red, *structure* in orange, *catenary wire* in cyan, and *LCG* in purple.

and reduces inference time by a third. We therefore deduce that ConvPoint offers a fair compromise between segmentation performance and training and inference speed.

Table 5: Network statistics.

Network	#parameters (million)	training time $\left(\frac{\text{GPU mins}}{\text{epoch}}\right)$	inference time $\left(\frac{\text{seconds}}{\text{scan}}\right)$
PointNet (Vanilla)	1.67	1.0	1.40
PointNet	3.53	1.2	1.47
PointNet++	0.97	6.5	2.91
PointNet++ (MSG)	1.88	7.8	3.71
RandLA-Net	1.30	6.8	5.80
ConvPoint	2.33	3.0	2.37

The mIoU values obtained with the network categorized as the best are 74.38% and 73.05% when using and obviating the intensity, respectively. These values are comparable with railway scene semantic segmentation works where metrics are calculated point-wise. For instance, in (Grandio et al., 2022), the test mIoU achieved by a modified PointNet++ architecture on the dataset presented in (Lamas et al., 2021) is 74.89%. Another example for comparison is the 77.3% mIoU value obtained with a novel deep-learning-based method (Manier et al., 2022) on Saint-Etienne dataset. Furthermore, compared to mIoU values presented in (Guo et al., 2021) for different architectures and benchmarks, our result is well above the average.

We assess our baseline methods robustness to varying point density by testing them with subsampled point clouds only at inference and compare their segmentation performances (see Figure 5). Although the grid size varies, the number of points per cube remains the same to have a fixed number of points per batch which makes the algorithm parallelizable. Therefore, a higher sampling grid size increases the redundancy of points in the input batches.

For sub-sampling grid resolutions lower than that used for training, all networks perform as good as in the initial testing phase, except for the case of using ConvPoint with intensity, where the test mIoU drastically drops from 74.38% to values under 34%. We notice that PointNet (Vanilla) is fairly robust under density decrease due to its focus on global abstraction rather than fine details. Interestingly, the segmentation performances of PointNet++ are less impaired by low point densities than PointNet++ (MSG). Moreover, for all grid sizes higher than 15cm, PointNet++ delivers one of the two best mIoU values among the networks.

In an industrial context, these robustness test results are particularly promising for PointNet++ taking into consideration the quantities of data that have to be processed. In fact, the inference protocol could be redesigned to perform on roughly subsampled scans using a much larger grid size to provide a fast global scene segmentation of very large data with a minimal loss of information e.g. for a fast count of catenary poles over long travelled distances.

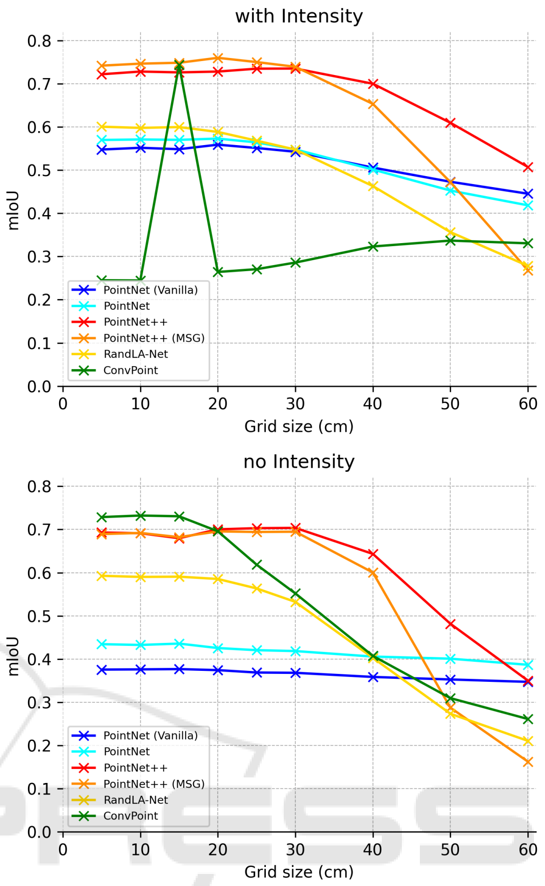

Figure 5: Effect of different grid-sampling resolutions with the test subset on the segmentation mIoU metric. The tested grid sizes are 5cm, 10cm, 15cm, 20cm, 25cm, 30cm, 40cm, 50cm, and 60cm.

5 CONCLUSION

In this paper, we presented a large-scale dataset showing unprecedented scale in point-wise annotation of railway scene point clouds. Baseline experiments were provided for semantic segmentation of point clouds from a single LiDAR scan. We experimented with four point-wise state-of-the-art architectures on our dataset. Our best baselines show similar segmentation results compared to other related baselines and outperforms the average results reported by benchmark studies on indoor or urban scene segmentation. Yet, there's still room for improvement of metric values obtained for railway-specific objects, and results are mitigated regarding training and inference times. Finally, the ability of some methods to process strongly subsampled scans without showing a severe drop in segmentation performance could meet industrial expectations in terms of speed for specific maintenance use cases.

Other than the complexity and size of our dataset, another possible reason for limited segmentation performance is that the point clouds captured by the rotating scanner are relatively sparse. It would therefore be feasible to test other methods like SPGraph (Landrieu and Simonovsky, 2018) that is less affected by distance-dependent sparsity, and SqueezeSeg (Wu et al., 2018) which exploits the way the LiDAR captures the data to generate a dense range image, where each pixel corresponds roughly to a point in the scan.

Future work also includes completing the dataset with additional data, compensating for the statistical class imbalance. Another development to further evaluate our baselines consists in segmenting more objects in order to annotate new classes such as fences, electrical cabinets and traffic lights. Besides, extending our experiments to classification and object detection tasks might be a promising direction for future research.

ACKNOWLEDGEMENTS

This research work contributes to the french collaborative project TASV (autonomous passenger-service train), with Railenium, SNCF, Alstom Crespin, Thales, Bosch and SpirOps. It was carried out in the framework of IRT Railenium, Valenciennes, France, and therefore was granted public funds within the scope of the French Program "Investissements d'Avenir".

REFERENCES

Abid, M. and Lefebvre, G. (2021). Improving indoor geomagnetic field fingerprinting using recurrence plot-based convolutional neural networks. *Journal of Location Based Services*, 15(1):61–87.

Behley, J., Garbade, M., Milioto, A., Quenzel, J., Behnke, S., Stachniss, C., and Gall, J. (2019). SemanticKITTI: A dataset for semantic scene understanding of LiDAR sequences. In *Proceedings of the IEEE/CVF international conference on computer vision*, pages 9297–9307.

Boulch, A. (2020). ConvPoint: Continuous convolutions for point cloud processing. *Computers & Graphics*, 88:24–34.

Choy, C., Gwak, J., and Savarese, S. (2019). 4D spatio-temporal convnets: Minkowski convolutional neural networks. In *Proceedings of the IEEE/CVF conference on computer vision and pattern recognition*, pages 3075–3084.

CloudCompare (2022). (version 2.12.2) [GPL software], retrieved from http://www.cloudcompare.org/.

Compagnon, P., Lomet, A., Reyboz, M., and Mermillod, M. (2023). Domestic hot water forecasting for individual housing with deep learning. In *Machine Learning and Principles and Practice of Knowledge Discovery in Databases*, pages 223–235.

Cordts, M., Omran, M., Ramos, S., Rehfeld, T., Enzweiler, M., Benenson, R., Franke, U., Roth, S., and Schiele, B. (2016). The cityscapes dataset for semantic urban scene understanding. In *Proceedings of the IEEE conference on computer vision and pattern recognition*, pages 3213–3223.

Everingham, M., Eslami, S. A., Van Gool, L., Williams, C. K., Winn, J., and Zisserman, A. (2015). The pascal visual object classes challenge: A retrospective. *International journal of computer vision*, 111:98–136.

Goyal, P., Dollár, P., Girshick, R., Noordhuis, P., Wesolowski, L., Kyrola, A., Tulloch, A., Jia, Y., and He, K. (2017). Accurate, large minibatch SGD: Training ImageNet in 1 hour. *arXiv preprint arXiv:1706.02677*.

Grandio, J., Riveiro, B., Soilán, M., and Arias, P. (2022). Point cloud semantic segmentation of complex railway environments using deep learning. *Automation in Construction*, 141:104425.

Guinard, S. A., Riant, J.-P., Michelin, J.-C., and Costa D'Aguiar, S. (2021). Fast weakly supervised detection of railway-related infrastructures in lidar acquisitions. *ISPRS Annals of the Photogrammetry, Remote Sensing and Spatial Information Sciences*, 2:27–34.

Guo, Y., Wang, H., Hu, Q., Liu, H., Liu, L., and Bennamoun, M. (2021). Deep learning for 3d point clouds: A survey. *IEEE Transactions on Pattern Analysis and Machine Intelligence*, 43(12):4338–4364.

Hackel, T., Savinov, N., Ladicky, L., Wegner, J. D., Schindler, K., and Pollefeys, M. (2017). Semantic3d. net: A new large-scale point cloud classification benchmark. *arXiv preprint arXiv:1704.03847*.

He, T., Zhang, Z., Zhang, H., Zhang, Z., Xie, J., and Li, M. (2019). Bag of tricks for image classification with convolutional neural networks. In *Proceedings of the IEEE/CVF conference on computer vision and pattern recognition*, pages 558–567.

Hu, Q., Yang, B., Xie, L., Rosa, S., Guo, Y., Wang, Z., Trigoni, N., and Markham, A. (2020). RandLA-Net: Efficient semantic segmentation of large-scale point clouds. In *Proceedings of the IEEE/CVF conference* *on computer vision and pattern recognition*, pages 11108–11117.

Kaijaluoto, R., Kukko, A., El Issaoui, A., Hyyppä, J., and Kaartinen, H. (2022). Semantic segmentation of point cloud data using raw laser scanner measurements and deep neural networks. *ISPRS Open Journal of Photogrammetry and Remote Sensing*, 3:100011.

Kölle, M., Laupheimer, D., Schmohl, S., Haala, N., Rottensteiner, F., Wegner, J. D., and Ledoux, H. (2021). The hessigheim 3d (h3d) benchmark on semantic segmentation of high-resolution 3d point clouds and textured meshes from uav lidar and multi-view-stereo. *ISPRS Open Journal of Photogrammetry and Remote Sensing*, 1:100001.

Lamas, D., Soilán, M., Grandío, J., and Riveiro, B. (2021). Automatic point cloud semantic segmentation of complex railway environments. *Remote Sensing*, 13(12):2332.

Landrieu, L. and Simonovsky, M. (2018). Large-scale point cloud semantic segmentation with superpoint graphs. In *2018 IEEE/CVF Conference on Computer Vision and Pattern Recognition*, pages 4558–4567.

Manier, A., Moras, J., Michelin, J.-C., and Piet-Lahanier, H. (2022). Railway lidar semantic segmentation with axially symmetrical convolutional learning. *ISPRS Annals of the Photogrammetry, Remote Sensing and Spatial Information Sciences*, 2:135–142.

Milioto, A., Vizzo, I., Behley, J., and Stachniss, C. (2019). RangeNet++: Fast and accurate lidar semantic segmentation. In *2019 IEEE/RSJ international conference on intelligent robots and systems (IROS)*, pages 4213–4220. IEEE.

Neuhold, G., Ollmann, T., Rota Bulo, S., and Kontschieder, P. (2017). The mapillary vistas dataset for semantic understanding of street scenes. In *Proceedings of the IEEE international conference on computer vision*, pages 4990–4999.

Qi, C. R., Su, H., Mo, K., and Guibas, L. J. (2017a). PointNet: Deep learning on point sets for 3D classification and segmentation. In *Proceedings of the IEEE conference on computer vision and pattern recognition*, pages 652–660.

Qi, C. R., Yi, L., Su, H., and Guibas, L. J. (2017b). PointNet++: Deep hierarchical feature learning on point sets in a metric space. *Advances in neural information processing systems*, 30.

Roynard, X., Deschaud, J.-E., and Goulette, F. (2018). Paris-lille-3d: A large and high-quality ground-truth urban point cloud dataset for automatic segmentation and classification. *The International Journal of Robotics Research*, 37(6):545–557.

Sergiyenko, O., Tyrsa, V., Zhirabok, A., and Zuev, A. (2023). Sliding mode observer based fault identification in automatic vision system of robot. *Control Engineering Practice*, 139:105614.

Soilán, M., Nóvoa, A., Sánchez-Rodríguez, A., Riveiro, B., and Arias, P. (2020). Semantic segmentation of point clouds with PointNet and KPConv architectures applied to railway tunnels. *ISPRS Annals of the Photogrammetry, Remote Sensing and Spatial Information Sciences*, 2:281–288.

Soilán, Sánchez-Rodríguez, Río-Barral, Perez-Collazo, Arias, and Riveiro (2019). Review of laser scanning technologies and their applications for road and railway infrastructure monitoring. *Infrastructures*, 4(4):58.

Thomas, H., Qi, C. R., Deschaud, J.-E., Marcotegui, B., Goulette, F., and Guibas, L. J. (2019). KPConv: Flexible and deformable convolution for point clouds. In *Proceedings of the IEEE/CVF international conference on computer vision*, pages 6411–6420.

Vallet, B., Brédif, M., Serna, A., Marcotegui, B., and Paparoditis, N. (2015). Terramobilita/iqmulus urban point cloud analysis benchmark. *Computers & Graphics*, 49:126–133.

Wu, B., Wan, A., Yue, X., and Keutzer, K. (2018). Squeezeseg: Convolutional neural nets with recurrent crf for real-time road-object segmentation from 3d lidar point cloud. In *2018 IEEE International Conference on Robotics and Automation (ICRA)*, pages 1887–1893.

Zhang, R., Candra, S. A., Vetter, K., and Zakhor, A. (2015). Sensor fusion for semantic segmentation of urban scenes. In *2015 IEEE international conference on robotics and automation (ICRA)*, pages 1850–1857.